A Distributed Approach to MPPT for PV Sub-Module Differential Power Processing

Shibin Qin, Stanton T. Cady, Alejandro D. Domínguez-García and Robert C.N. Pilawa-Podgurski

Department of Electrical and Computer Engineering

University of Illinois at Urbana-Champaign, Urbana, Illinois, USA

E-mail: {sqin3, scady2, aledan, pilawa}@ILLINOIS.EDU

***Abstract*—This paper presents a distributed control algorithm for differential power processing in photovoltaic (PV) applications. This distributed algorithm performs *true* maximum power point tracking (MPPT) of series-connected PV sub-modules with only neighbor-to-neighbor communication and local measurements of each differential power converter voltages, obviating the need for local current measurements. Reduced number of perturbations at each step and potentially faster tracking can be achieved compared to previous solutions, while no extra hardware is required, all of which make this algorithm well-suited for long sub-module strings. The formulation of the control algorithm as well as three case studies are presented; both simulations and hardware experiments have confirmed the effectiveness of the proposed distributed algorithm.**

I. Introduction

In photovoltaic (PV) energy systems, PV modules are often connected in series for increased string voltage; however, I-V characteristics mismatches often exist between series connected PV modules, typically as a result of partial shading, manufacturing variability and thermal gradients. Since all modules in a series string share the same current, the overall output power can be limited by underperforming modules. A bypass diode is often connected in parallel with each PV module to mitigate this mismatch and prevent PV hot spotting, but the efficiency loss is still significant when only a central converter is used to perform MPPT on the PV string.

To address the mismatch problem, distributed power electronics that perform module-level or even sub-module-level MPPT have been proposed. The two most dominant solutions are DC optimizers [1]–[4], and micro-inverters [5]–[7]. The major limitation of these two solutions, however, is that distributed converters must process the full power output of every module or sub-module. Even with highly efficient distributed converters, the overall power losses of the system can still be significant.

Differential power processors (DPPs) have gained significant attention recently due to its substantial improvements over conventional solutions in terms of efficiency, reliability, and cost. A high level introduction to the DPP concept can be found in [8]. In contrast to DC optimizers or micro-inverters, DPPs only need to process the power difference between series connected PV modules, which is often just a small fraction of the bulk power. This results in high system efficiency, small size and reduced power ratings of the power electronics circuit components.

To apply the concept of differential power processing to PV systems, especially at the sub-module level, several architectures and corresponding control schemes have been proposed [9]–[14]. For example, the work presented in [13] uses a switched inductor topology, the work presented in [11] uses a resonant switched capacitor topology, while the work presented in [12] uses a transformer coupled topology. All of them adopt a control method commonly known as voltage equalization or "virtual parallel" operation, in which all distributed converters strive to equalize the voltages of all PV sub-modules in a string. The distributed converters in the system run in open loop, simplifying the control requirements while obviating the need for communication among converters. However, the voltage equalization approach can only achieve *near* maximum power point (MPP) operation without truly seeking the MPP of each individual sub-module. The effectiveness of this approach relies on the fact that the MPP voltages of sub-modules in a string are very close, requiring all the sub-modules to have very similar electrical characteristics. This is typically guaranteed by a costly binning process performed by PV module manufacturers [15]. Even modules that are carefully matched at installation, however, will suffer from non-uniform degradation after several years of field exposure. As shown in [16], the standard deviation of PV module MPP voltages increased nearly four times over twenty years. Furthermore, field operating conditions such as thermal gradient or severe insolation mismatch along the PV string can also cause the MPP voltages of sub-modules to drift apart. All of these factors limit the tracking efficiency of the voltage equalization approach; thus, in order to increase the total energy harvested over the entire lifetime of the PV system, it is necessary to develop a scheme capable of true MPPT.

The information, data, or work presented herein was funded in part by the Advanced Research Projects Agency-Energy (ARPA-E), U.S. Department of Energy, under Award DE-AR0000217.

On the other hand, the generation control circuit presented in [9], [10] achieves true MPPT without any local current sensing at each sub-module, but employs a control scheme that requires communication between all converters and a central control unit. The central control unit has to command all the distributed converters to exhaust every possible combination of converter duty ratio perturbations and measure the string voltage respectively in sequence before making the next tracking step. For a system with n DPPs, 2^n possible combinations of perturbations have to be tried during each tracking step, rendering the algorithm slow and infeasible for a large system. Moreover, with this approach, the reliability of the system is fundamentally limited, as the single point of failure of the central control unit or a communication link would result in the failure or malfunction of the overall system. The work presented in [14] adopts a buck-boost converter topology that overcomes some of the limitations in the architecture of the generation control circuit, and achieves true MPPT with a faster control scheme. However, this control scheme still requires communication between all DPPs and the central converter.

In this paper, we seek to overcome the limitations discussed above through the use of a distributed algorithm that requires only *neighbor-to-neighbor* communication between adjacent DPPs to perform sub-module-level *true* MPPT. In our approach, there is *no* need for a central control unit or any local current sensing at each converter. Instead, each DPP only perturbs its duty ratio once per tracking step, and observes only local voltage changes (instead of the entire string voltage). Moreover, the algorithm has the potential for parallelization of the duty ratio perturbations as the sensitivity between non-adjacent DPPs is low, which can reduce the communication overhead and speed up the tracking even further. Compared to the centralized approach, no extra hardware is needed since the algorithm can be implemented in the micro-controller of each DPP that already exist for the DPP's local control. Furthermore, since a central control unit is unnecessary and each micro-controller can make independent control decisions, there is no longer a single point of failure, increasing the overall system reliability.

The remainder of this paper is organized as follows. The formulation of the distributed MPPT algorithm is presented in Section II. Hardware implementation of the DPPs and the experiment setup used to verify the MPPT algorithm are introduced in Section III. Section IV provides case studies involving a 3-DPP system, and a 5-DPP system, including both simulation and experimental results, followed with simulation results for a larger 31-DPP system. Finally, Section V concludes the paper.

II. MPPT Algorithm Formulation

In this section, we formulate a distributed iterative control algorithm which, through the exchange of information among local controllers, and for a given string current, maximizes the power extracted from an array of n series-connected PV sub-modules outfitted with $n-1$ DPP converters. We first formulate the algorithm for a 3-sub-module, 2-DPP system, and then generalize it to a system of any size.

A system comprised of two DPP converters and three sub-modules is illustrated in Fig. 1. This system is based on the architecture presented in [14]. Each DPP is implemented as a buck-boost converter that enforces a voltage ratio between two PV sub-modules. The PV string is attached to a central converter (omitted in Fig. 1). The central converter is configured as a controllable current sink, and seeks the optimal string current in a relatively slow perturb and observe (P&O) control loop. Because the perturb interval of the central converter is much longer than the DPP local control loop's time constant, at any given time, the string current can be considered temporarily fixed for the DPPs. Given a fixed string current, I_o, it is easy to see that, regardless of the irradiance incident on each of the sub-modules, maximizing the string voltage, $V := V_1 + V_2 + V_3$, is equivalent to maximizing the power extracted from the system. Furthermore, in our setting, we observe that each DPP converter has access to measurements of only two of the three sub-module voltages. Thus, in order to determine the duty ratios for which V is maximized, we assume that the local controllers of DPP_1 and DPP_2 can share information as illustrated by the directed graph to the right of the block diagram in Fig. 1. To this end, we tailor the distributed optimization algorithm in [17] to our setting.

The control objective described above can be written as

$$\max V(D_1, D_2) = V_1(D_1, D_2) + V_2(D_1, D_2) + V_3(D_1, D_2),$$

where D_1 and D_2 are the duty ratios of DPP_1 and DPP_2, respectively. Then, the maxima of the function $V(D_1, D_2)$ can by found by setting its gradient to zero, as in (1) at the bottom of this page, where D_1^* and D_2^* are the respective duty ratios of DPP_1 and DPP_2 at the maximum power point. To find D_1^* and D_2^*, the local controller of each DPP iteratively adjusts its duty ratio based on local measurements as well as state variables maintained locally and by the neighboring DPP(s). Let $k = 1, 2, \ldots$ index the iterations performed by each DPP converter, and let $D_1[k]$, $D_2[k]$ be the the duty ratio of DPP_1 and DPP_2, $\hat{D}_2[k]$, $\hat{D}_1[k]$ be an estimate of the neighboring DPP's duty ratio for DPP_1 and DPP_2, respectively. Furthermore, let $z_{1,i}[k]$, and $z_{2,i}[k]$, $i = 1, 2$, be ancillary state variables maintained by

$$\nabla V(D_1^*, D_2^*) = \begin{bmatrix} \left.\frac{\partial V_1(D_1,D_2)}{\partial D_1}\right|_{D_1^*,D_2^*} + \left.\frac{\partial V_2(D_1,D_2)}{\partial D_1}\right|_{D_1^*,D_2^*} + \left.\frac{\partial V_3(D_1,D_2)}{\partial D_1}\right|_{D_1^*,D_2^*} \\ \left.\frac{\partial V_1(D_1,D_2)}{\partial D_2}\right|_{D_1^*,D_2^*} + \left.\frac{\partial V_2(D_1,D_2)}{\partial D_2}\right|_{D_1^*,D_2^*} + \left.\frac{\partial V_3(D_1,D_2)}{\partial D_2}\right|_{D_1^*,D_2^*} \end{bmatrix} = \begin{bmatrix} 0 \\ 0 \end{bmatrix} \tag{1}$$

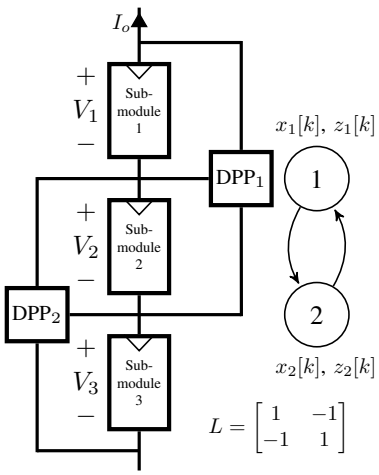

Fig. 1. Block diagram of 3-sub-module, 2-DPP system.

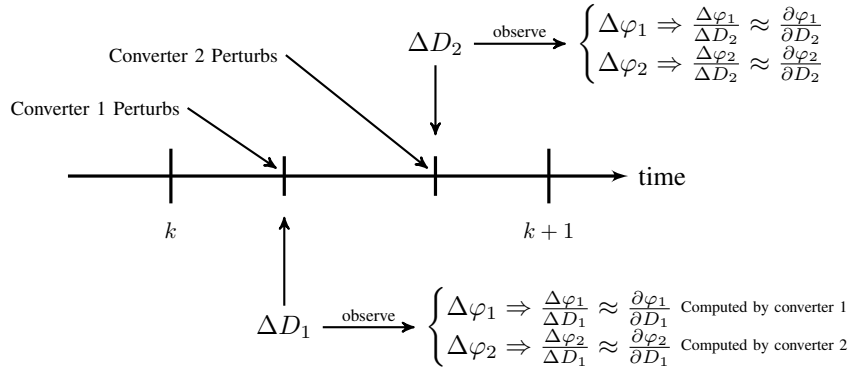

Fig. 2. Timeline of distributed perturb and observe.

the local controllers, and define

$$x[k] = \big[\underbrace{D_1[k], \hat{D}_2[k]}_{x_1[k]}, \underbrace{\hat{D}_1[k], D_2[k]}_{x_2[k]}\big]^{\mathrm{T}}, \tag{2}$$

$$z[k] = \big[\underbrace{z_{1,1}[k], z_{1,2}[k]}_{z_1[k]}, \underbrace{z_{2,1}[k], z_{2,2}[k]}_{z_2[k]}\big]^{\mathrm{T}}. \tag{3}$$

Then, at each iteration, the variables are updated as

$$x[k+1] = (\mathbb{I}_4 - \delta\tilde{L})x[k] - \delta\tilde{L}z[k] + \delta\gamma u[k], \tag{4}$$

$$z[k+1] = z[k] + \delta\tilde{L}x[k], \tag{5}$$

where $\mathbb{I}_4$ is the 4×4 identity matrix; $\tilde{L} = L \otimes \mathbb{I}_2$, where $\mathbb{I}_2$ is the 2×2 identity matrix, and L is the Laplacian of the graph representing the exchange of information between local controllers as given in Fig. 1; δ and γ are variables that can be used to tune the algorithm; and $u[k]$ is defined in (6) at the bottom of this page, with φ_1 and φ_2 defined respectively as

$$\varphi_1(D_1, D_2) := V_1(D_1, D_2) + \frac{1}{2}V_2(D_1, D_2),$$

$$\varphi_2(D_1, D_2) := \frac{1}{2}V_2(D_1, D_2) + V_3(D_1, D_2).$$

From the above discussion, we see that the update of DPP$_1$'s states depends on its own states, the states of its neighbor and the partial derivatives of the sub-module voltages that DPP$_1$ is directly attached to. While (4) and (5) conform to the exchange of information between neighbors and rely only on directly accessible measurements for each DPP, in order to obtain $u_i[k]$, $i = 1, 2$, each DPP must estimate the partial derivatives of their respective $\varphi(\cdot)$ functions. To acquire these estimates, at every iteration, each DPP alternatively perturbs its duty ratio while both local controllers observe the sub-module voltages as illustrated by the timeline in Fig. 2. After both local controllers have observed the results of each perturbation, they can approximate the partial derivatives as $\frac{\partial\varphi_i}{\partial D_j} \approx \frac{\Delta\varphi_i}{\Delta D_j}$, $i, j = 1, 2$; upon receiving the necessary information from the neighboring DPP, they compute the updates for their respective state variables. After $k = m$ iterations, for m sufficiently large, we have that $D_1[m] \approx D_1^*$ and $D_2[m] \approx D_2^*$; thus the string voltage is maximized and the maximum power is extracted from the system.

For a system of n sub-modules and $n-1$ DPP converters, we use the same update equations given in (4) and (5) with $\mathbb{I}_{(n-1)^2}$ instead of $\mathbb{I}_4$, and $\tilde{L} = L \otimes \mathbb{I}_{n-1}$ instead of $L \otimes \mathbb{I}_2$, where now L is the Laplacian of a graph similar to that in Fig. 1 but with $n-1$ nodes:

$$L = \begin{bmatrix} 1 & -1 & 0 & \dots & \dots & 0 \\ -1 & 2 & -1 & 0 & \dots & 0 \\ 0 & -1 & 2 & -1 & \ddots & \vdots \\ \vdots & \ddots & \ddots & \ddots & \ddots & \vdots \\ \vdots & \ddots & \ddots & -1 & 2 & -1 \\ 0 & \dots & \dots & \dots & -1 & 1 \end{bmatrix}.$$

Furthermore, each local controller will maintain an estimate of the duty ratios of all other DPPs in addition to its own; thus, DPP$_i$ maintains $D_i[k]$ and $\hat{D}_j[k]$, $i, j = 1, \dots, n-1$, $i \neq j$. Similar to the two-DPP case, we define

$$x[k] = \begin{bmatrix} x_1[k] & x_2[k] & \dots & x_{n-1}[k] \end{bmatrix}^{\mathrm{T}},$$

$$z[k] = \begin{bmatrix} z_1[k] & z_2[k] & \dots & z_{n-1}[k] \end{bmatrix}^{\mathrm{T}},$$

$$u[k] := \Bigg[\overbrace{\frac{\partial\varphi_1}{\partial D_1}\bigg|_{D_1[k],D_2[k]}, \frac{\partial\varphi_1}{\partial D_2}\bigg|_{D_1[k],D_2[k]}}^{u_1[k] = \frac{\partial\varphi_1(D)}{\partial D}}, \overbrace{\frac{\partial\varphi_2}{\partial D_1}\bigg|_{D_1[k],D_2[k]}, \frac{\partial\varphi_2}{\partial D_2}\bigg|_{D_1[k],D_2[k]}}^{u_2[k] = \frac{\partial\varphi_2(D)}{\partial D}}\Bigg]^{\mathrm{T}} \tag{6}$$

where $x_i[k]$ and $z_i[k]$, $i = 1, 2, \ldots, n-1$ are actually not individual elements of $x[k]$ but rather a representation of the collection of states kept by the ith DPP, i.e.,

$$x_i[k] = \left[\hat{D}_1[k], \ldots, \hat{D}_{i-1}[k], D_i[k], \hat{D}_{i+1}[k], \ldots, \hat{D}_{n-1}[k]\right]^{\mathrm{T}},$$
$$z_i[k] = \left[z_{i,1}[k], z_{i,2}[k], \ldots, z_{i,n-1}[k]\right]^{\mathrm{T}}.$$

We also define

$$u[k] = \left[\frac{\partial\varphi_1(D)}{\partial D} \quad \frac{\partial\varphi_2(D)}{\partial D} \quad \ldots \quad \frac{\partial\varphi_{n-1}(D)}{\partial D}\right]^{\mathrm{T}}, \tag{7}$$

where

$$\frac{\partial\varphi_i(D)}{\partial D} = \left[\frac{\partial\varphi_i(D)}{\partial D_1}, \frac{\partial\varphi_i(D)}{\partial D_2}, \ldots, \frac{\partial\varphi_i(D)}{\partial D_{n-1}}\right]^{\mathrm{T}}, \tag{8}$$

with $\varphi_i(D)$ given by

$$\varphi_i(D) = \begin{cases} V_i(D) + \frac{1}{2}V_{i+1}(D), & i = 1 \\ \frac{1}{2}V_i(D) + \frac{1}{2}V_{i+1}(D), & 1 < i < n-1 \\ \frac{1}{2}V_i(D) + V_{i+1}(D) & i = n-1. \end{cases} \tag{9}$$

By inspecting (4) and (5) for the n-sub-module case, it is easy to see that the state of the ith DPP at instant $k+1$, $x_i[k+1]$, depends on its own state at instant k, $x_i[k]$; the states of its neighboring DPPs at instant k, i.e., $x_{i-1}[k]$, $z_{i-1}[k]$, $x_{i+1}[k]$, $z_{i+1}[k]$, all of which can be acquired through the neighbor-to-neighbor communication; and $u_i[k]$, which is approximated by the ith DPP as $\frac{\Delta\varphi_i(D)}{\Delta D}$. Similar to the 2-DPP case, after $k = m$ iterations, for m sufficiently large, we have $D_i[m] \approx D_i^*, i = 1, 2, \ldots, n-1$.

III. Laboratory Testbed

In this section, a brief introduction to the DPP hardware design is provided, followed by a description of the experimental setup used to verify the proposed algorithm.

A. DPP Hardware Implementation

Figure 3 illustrates the wire connection of a DPP system; typically one PV module consists of three sub-modules. Therefore, each junction box needs to integrate three DPPs. Between adjacent junction boxes there are three wire connections: one series string connection in which the bulk power common to all sub-modules flows, one differential connection through which the DPPs shuffle the small power mismatch, and one or more wires for communication.

In this work, DPPs are implemented as bidirectional synchronous buck-boost converters. As analyzed in [14], the buck-boost topology allows for the use of low-voltage, fast-switching transistors. By employing a fast switching frequency in the order of hundreds of kHz, the size of magnetic component can be reduced. Furthermore, while in [14] each DPP has one dedicated micro-controller, each micro-controller has enough peripherals to control more than one DPP. Since the 3 DPPs in one junction box are physically very close, they can be integrated on one printed circuit board (PCB) and controlled by one micro-controller. This eliminates the need for communication between DPPs in one junction box and reduces the control overhead in terms of hardware cost and power consumption. For this work, we chose a 32-bit ARM Cortex-M3 micro-controller, which allows some flexibility for future expansions, e.g., implementation of fault detection algorithm. Each DPP is constructed with a shielded power inductor and an integrated DrMOS power stage to achieve high efficiency and very small footprints on PCB.

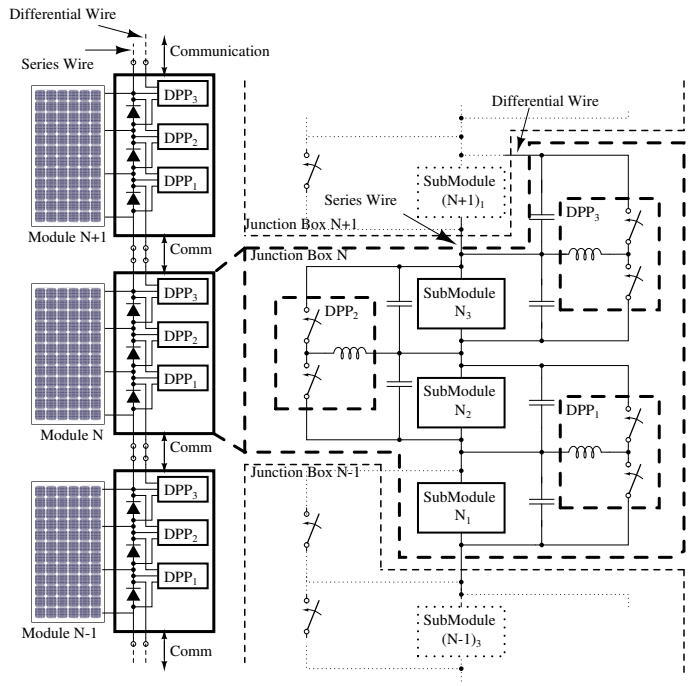

Fig. 3. PV junction box connection for DPP system.

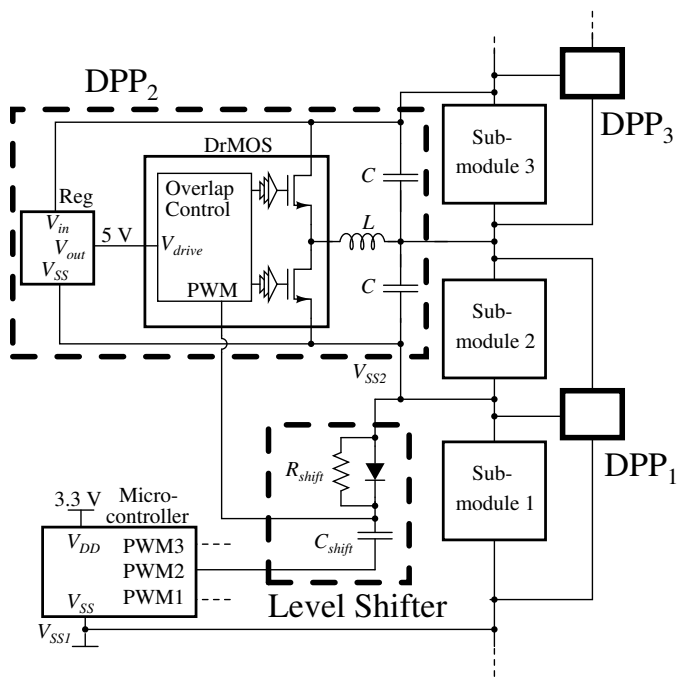

Fig. 4. Detail Schematic of hardware design (details shown for DPP_2 only).

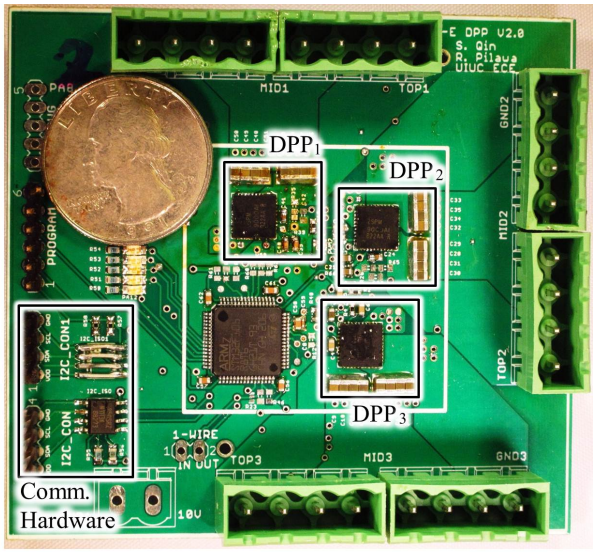

Fig. 5. Photograph of the hardware prototype with a US quarter for scale.

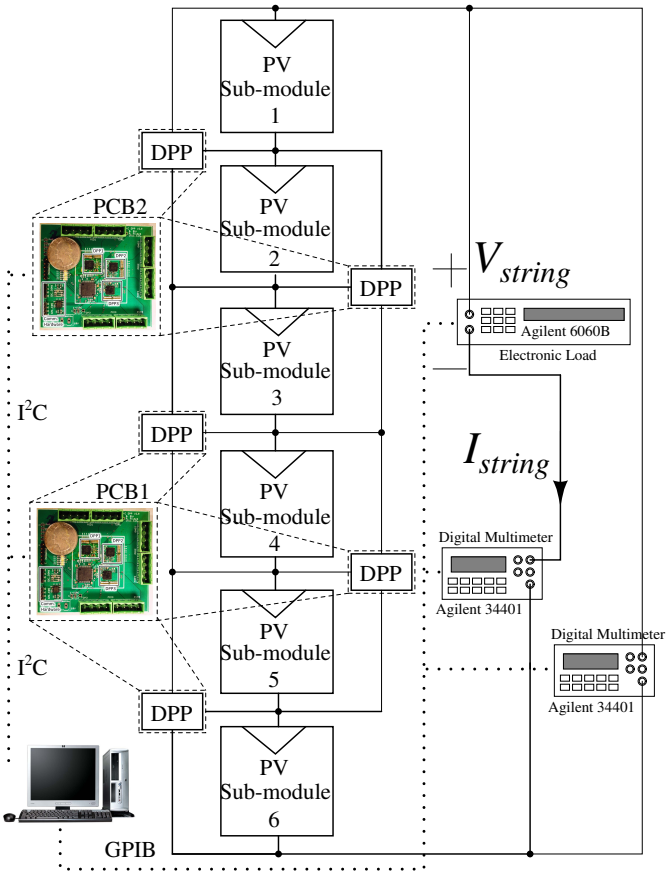

Fig. 6. Experimental setup.

One unique challenge of controlling 3 DPPs with one micro-controller is sending control signal across different voltage levels. While DDP_1 can be controlled directly by the micro-controller, PWM control signals to DPP_2 and DPP_3 must be level shifted because they do not share the same ground reference with the micro-controller, as shown in Fig. 4. This figure illustrates the circuit details for DPP_2 only, while those for DPP_1 and DPP_3, which are similar, are omitted. A simple diode-capacitor level shifter is chosen in our design to reduce the cost and size, and proves to be working well. A list of the main hardware components used is provided in Table I.

TABLE I
MAIN COMPONENT LIST

Device	Model	Value	Manufacturer
Microcontroller	STM32F105		STMicroelectronics
DrMOS	SiC780		Vishay
Linear Regulator	UA78L05CPK		Texas Instrument
L	SER1360-103KL	10 μH	Coilcraft
C	TMK212BBJ106KG-T	10 μF$\times$4	Taiyo Yuden
D_{shift}	1SS416CT(TPL3)		Toshiba
C_{shift}	0402	$4700pF$	
R_{shift}	0402	100 kΩ	
I^2C Isolator	ADuM1250		Analog Devices

TABLE II
HARDWARE PROTOTYPE SPECIFICATIONS

Sub-module Voltage Range	3-13 V
Converter Power Rating	60 W
Switching Frequency	100 kHz
Duty Ratio Resolution (with Duty Ratio Dithering Technique [18], [19])	1/3600
Converter Peak Efficiency	95%
Weight	28 grams
Volume	8.575 cm^3

Figure 5 shows an annotated photograph of the front side of the hardware prototype. Magnetic inductors are on the back side of the PCB. Note that a large portion of the board area is consumed by large connectors and ancillary circuits to facilitate development and diagnosis, which can be eliminated in the final product. As shown in Fig. 5, all essential components of the hardware, including the inductors on the back side of the PCB, only take up a 3.75 cm$\times$3.75 cm area encompassed by a white rectangle, and can easily fit in a junction box. Table II list specifications of the hardware prototype.

B. Experimental Setup

To verify the proposed MPPT algorithm, we developed the indoor experimental setup in Fig. 6. A power supply (HP 6631A) was connected in parallel with each PV sub-module to replicate the photovoltaic current, providing an output I-V characteristic as if the PV sub-module was illuminated by sunlight. Details about this method to conduct repeatable indoor PV experiment can be found in [20]. Five DPPs implemented on 2 prototype boards were connected in parallel with a string of six PV sub-modules. Three of them are Sunmodule^{TM} SW 235 Poly PV modules and the other three are SW 245 Poly PV modules. The two modules of the same series are manufactured in the same process but binned into two different type to mitigate the characteristic variation. In this setup, they are chosen intentionally to emulate PV modules undergoing a less stringent binning process. An electronic load (Agilent

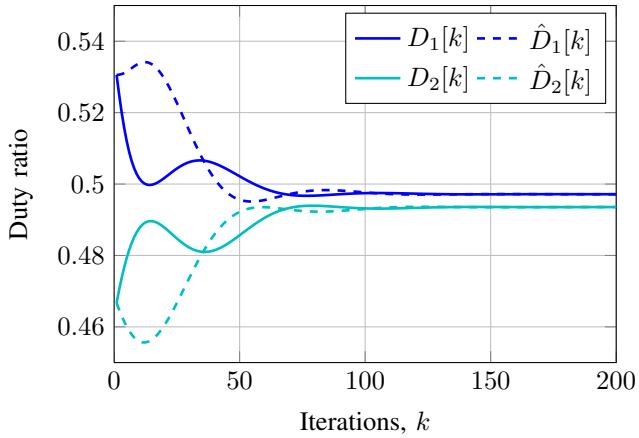

Fig. 7. Evolution of duty ratios computed by distributed algorithm for 2-DPP simulation with insolation pattern of 100%, 80%, 50%, $I_{string} = 3.3A$, $\delta = 0.1$ and $\gamma = 0.003$.

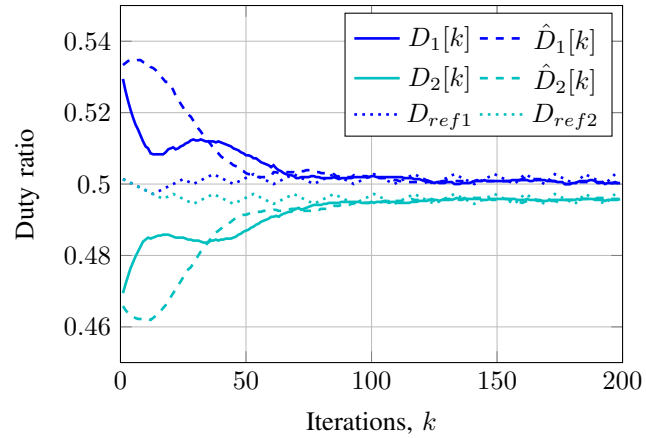

Fig. 8. Evolution of duty ratios computed by distributed algorithm for 2-DPP experimental setup with insolation pattern of 100%, 80%, 50%, $I_{string} = 3.3A$, $\delta = 0.1$ and $\gamma = 0.003$. Evolution of the centralized algorithm proposed in [14] is also plotted in dotted lines as a reference for the final value after converge.

6060B) acted as a central converter and controlled the string current. Two digital multimeters (Agilent 34401) were used to measure the string voltage and current. All power supplies, digital multimeters and the electronic load communicated with a computer through a GPIB interface. Micro-controllers on the two prototype boards communicated with each other and with the same computer through an I^2C interface. Note that for the following tests of the proposed distributed algorithm, the computer only received information from micro-controllers for data logging and diagnostic purposes. The distributed algorithm, including data exchange and synchronization at each iteration, is implemented in the micro-controllers.

In the experiment, the current limits of the power supplies were set to certain percentage of the sub-modules' nominal short circuit current to emulate the corresponding percentage of insolation (e.g., 5A, 4A and 2.5A to emulate a 100%, 80% and 50% insolation situation). For a given insolation mismatch scenario, a string current sweep was conducted by the electronic load. During each sweep step, the string current was kept fixed for the algorithm to converge to a steady state. The evolution of duty ratios of all DPPs, along with the string current and voltage after the algorithm's convergence was recorded by the computer.

IV. Case Studies

In this section we verify the efficacy of the proposed distributed algorithm through three case studies. We first present and compare simulation and experimental results from the simplest 2-DPP system to illustrate its basic characteristics. Then, we focus on the experimental result of a six-sub-module 5-DPP system and analyze its tracking efficiency. Finally, we demonstrate the scalability of the algorithm by presenting simulation results for a system containing 31-DPP converters and 32 sub-modules.

A. 2 Differential Power Processors

To study the simplest 2-DPP case, we conducted experiments on the setup discussed in Section III but with only 3 sub-modules and compared the data with a MATLAB simulation. We set the conditions (i.e., insolation pattern, string current and initial duty ratios) to be the same in experiment and simulation, and recorded the evolution of the states of the algorithm. This test was performed for different conditions, and we found good matching between simulation and experimental data. Figure 7 shows one example of the evolution of the duty ratios of a simulated system with $100\%, 80\%, 50\%$ insolation on sub-modules 1,2 and 3, respectively. The string current was set to MPP current that corresponds to this condition. Figure 8 shows the evolution of the duty ratios computed using the experimental setup with the same condition. As the figures show, the state variables in both the simulations and experiments quickly reach convergence and follow roughly the same trajectory, and the duty ratios $D_1[k]$ and $D_2[k]$ settle to the same value as corresponding duty ratio estimates $\hat{D}_1[k]$ and $\hat{D}_2[k]$. To verify that the algorithm converges to the correct value, on the experimental setup, we also executed the centralized MPPT algorithm in [14], and record its duty ratio evolution as a benchmark (i.e., D_{ref1} and D_{ref2} in Fig. 8). The final duty ratios of the proposed algorithm are almost identical to those of the centralized MPPT algorithm. Tests of other insolation patterns and string current exhibit similar results, and are omitted due to space limitations.

B. 5 Differential Power Processors

Similar to the 2-DPP case, we tested the proposed algorithm on a 5-DPP system for different conditions. Figures 9 and 10 show one example of the simulation and experimental result for the same conditions and initial duty ratios. Note that among all the state variables, only the actual duty ratios $D_i[k], i = 1, 2, \ldots, 5$, are plotted, and all $\hat{D}_i[k], i = 1, 2, \ldots, 5$ are omitted. Along with the distributed MPPT algorithm, the centralized MPPT algorithm proposed in [14] is also executed, and its evolution is plotted in Fig. 10 as a benchmark. Note that in both 2-DPP and 5-DPP case, states in simulation and experiment follow very similar trajectories but do not converge to exactly the same final values, primarily due to two reasons.

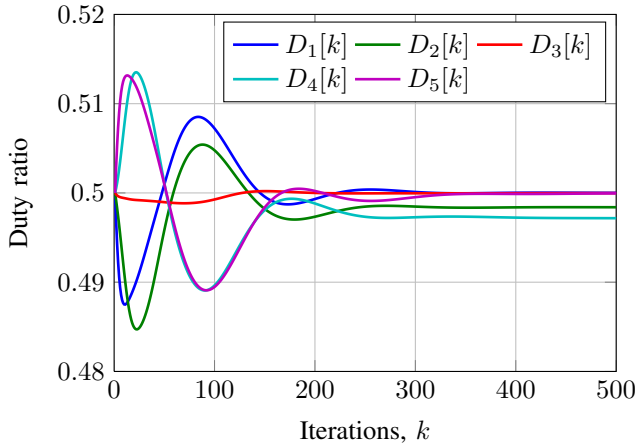

Fig. 9. Evolution of duty ratios computed by distributed algorithm for 5-DPP simulation with insolation pattern of 100%, 100%, 80%, 80%, 50%, 50%, $I_{string} = 3.3A$, $\delta = 0.1$ and $\gamma = 0.002$.

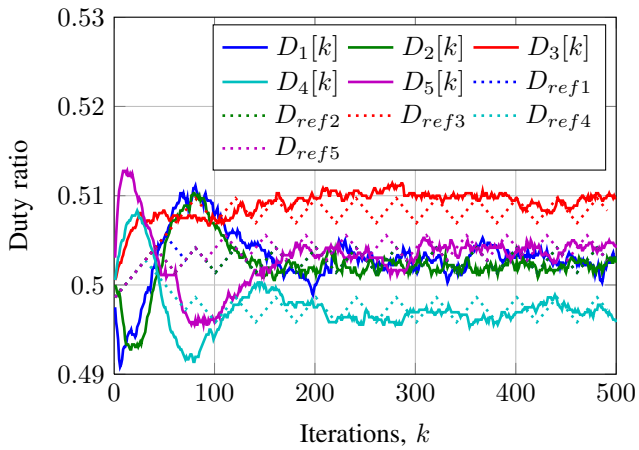

Fig. 10. Evolution of duty ratios computed by distributed algorithm for 5 -DPP experimental setup with insolation pattern of 100%, 100%, 80%, 80%, 50%, 50%, $I_{string} = 3.3A$, $\delta = 0.1$ and $\gamma = 0.002$. Evolution of the centralized algorithm proposed in [14] is also plotted in dotted lines as a reference for the final value after converge.

First, the simulation does not take into account the converter power losses. Second, as we used two types of PV modules in the experiment to emulate modules with less stringent binning, there is some variation in the I-V curves of the six sub-modules, which is not captured in the simulation.

At the same time, it is evident that the proposed algorithm and the centralized MPPT algorithm converge to the same final value. However, due to the noise in the voltage measurements, the duty ratio values still have small variations after convergence. With smaller value of γ in (4), the steady state variation can be significantly reduced as $D_i[k]$ is less dependent on $u_i[k]$, but the algorithm will take more iterations to converge to the steady state, as shown in Fig. 11. In terms of hardware related issues, the noise in the voltage measurements can be reduced by averaging multiple reading or filtering with larger capacitors at the ADC pins. However, both of these methods will increase the time needed for each iteration, and slow down the convergence of the algorithm. Similar to γ, the value of δ

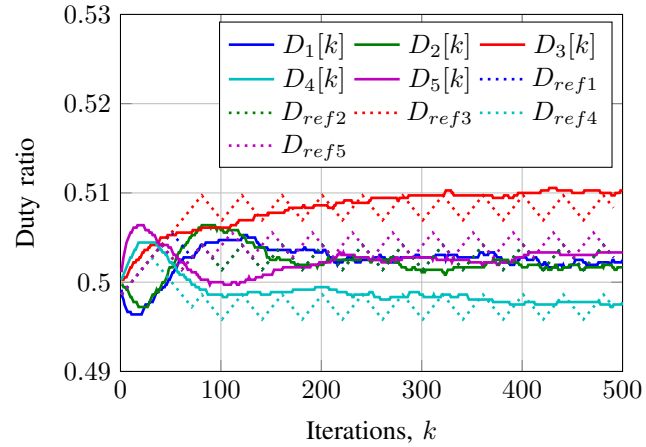

Fig. 11. Evolution of duty ratios computed by distributed algorithm for 5-DPP experimental setup with insolation pattern of 100%, 100%, 80%, 80%, 50%, 50%, $I_{string} = 3.3A$, $\delta = 0.1$ and $\gamma = 0.0004$. Evolution of the centralized algorithm proposed in [14] is also plotted in dotted lines as a reference for the final value after converge.

in (4) and (5) can also be increased to speed up the algorithm. However, δ represents a trade-off between speed and stability of the algorithm. Because the system is highly non-linear, δ can only be determined empirically, and we found δ should be kept smaller than 0.1 to guarantee stability in most situations. To further verify that the proposed algorithm effectively tracks the maximum power point, voltages of the six sub-modules were measured after the algorithm reaches steady state, and compared with the experimentally measured maximum power point voltage of each sub-module. The measured sub-module voltages were projected back to the measured I-V curve of that sub-module to find the operating point of the sub-module, and a tracking efficiency was calculated based on the power at this operating point and the MPP power. The results for a few different scenarios are displayed in Table III.

C. 31 Differential Power Processors

To demonstrate the scalability of the distributed MPPT algorithm, we extended the simulation to model a system with 32 sub-modules and 31 DPPs. The evolution of the duty ratios found by each of the DPP local controllers using the distributed algorithm is shown in Fig. 12 for randomly chosen initial conditions and for an insolation pattern in which all sub-modules receive 100% irradiance. As Fig. 12 shows, the algorithm converges to the expected solution wherein the duty ratios are $D_i = 0.5$, $i = 1, \ldots, n-1$. While more iterations are required for larger system to converge from a random initial point, an in-depth study of the system reveals that the algorithm can use a small γ value at start-up to prevent excessive duty ratio oscillation. Once the algorithm converges, γ can be changed to a large value for fast response. Moreover, some of the terms in $u_i[k]$ as defined in (8), $\frac{\partial \varphi_i(D)}{\partial D_j} \approx \frac{\Delta \varphi_i(D)}{\Delta D_j}$, are effectively zero when i and j are far apart. This allows parallelization of DPP duty ratio perturbations to speed up the convergence. Details about the optimization of this algorithm are omitted due to space limitations.

TABLE III
FINAL DUTY RATIO COMPARISON

Insolation Patter	100%, 100%, 80%, 80%, 50%, 50%	100%, 100%, 100%, 100%, 100%, 100%	100%, 100%, 100%, 80%, 80%, 80%
Centralized MPPT Duty Ratio	0.503, 0.503, 0.508, 0.497, 0.503	0.499, 0.500, 0.502, 0.496, 0.501	0.501, 0.501, 0.504, 0.499, 0.502
Distributed MPPT Duty Ratio	0.502, 0.502, 0.510, 0.497, 0.504	0.499, 0.499, 0.502, 0.496, 0.501	0.501, 0.501, 0.505, 0.499, 0.501
Operating Point Voltage (V)	10.032, 10.127, 9.859, 10.081, 9.478, 9.461	9.960, 10.045, 9.953, 10.224, 10.229, 10.135	10.007, 10.035, 10.027, 9.991, 10.022, 9.883
MPP Voltage (V)	10.080, 10.092, 9.901, 10.124, 9.694, 9.783	10.080, 10.092, 10.021, 10.289, 10.236, 10.292	10.080, 10.092, 10.021, 10.124, 10.057, 10.127
Tracking efficiency	99.97%, 99.98%, 99.99%, 99.97%, 99.70%, 99.50%	99.95%, 99.95%, 99.98%, 99.97%, 99.99%, 99.93%	99.97%, 99.95%, 99.99%, 99.94%, 99.97%, 99.73%

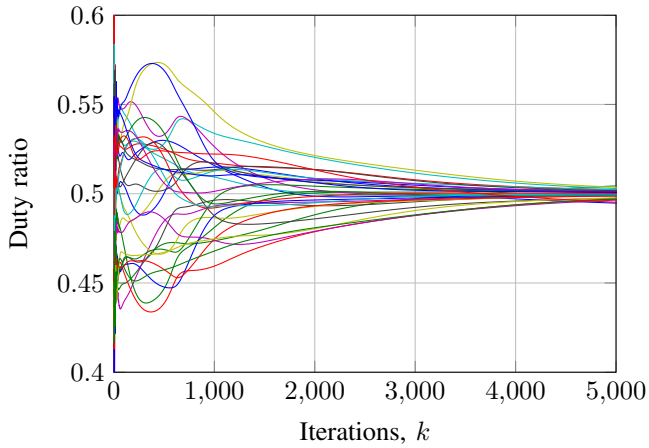

Fig. 12. Evolution of duty ratios computed by distributed algorithm for 31 -DPP simulation with 100% insolation on all sub-modules and random initial duty ratios.

V. CONCLUSIONS

In this paper, we addressed the problem of maximizing the power extracted from a system of series-connected PV modules outfitted with DPPs. To tackle some of the drawbacks of previously proposed centralized MPP algorithms, we introduced a distributed perturb and observe algorithm which relies on neighbor-to-neighbor communication and requires only local voltage measurements. Hardware suitable for PV junction box integration was developed. To verify the efficacy of the proposed algorithm, we presented simulation and experimental results for a 2-DPP and a 5-DPP system. We then demonstrated the scalability of the algorithm by presenting results for a 31-DPP system.

REFERENCES

[1] G. R. Walker and P. C. Sernia, "Cascaded dc-dc converter connection of photovoltaic modules," *IEEE Transaction on Power Electronics*, vol. 19, no. 4, pp. 1130–1139, 2004.

[2] N. Femia, G. Lisi, G. Petrone, G. Spagnuolo, and M. Vitelli, "Distributed maximum power point tracking of photovoltaic arrays: Novel approach and system analysis," *IEEE Transactions on Industrial Electronics*, vol. 55, no. 7, pp. 2610–2621, 2008.

[3] L. Linares, R. Erickson, S. MacAlpine, and M. Brandemuehl, "Improved energy capture in series string photovoltaics via smart distributed power electronics," in *Proc. of the Applied Power Electronics Conference and Exposition*, pp. 904–910, 2009.

[4] R. Pilawa-Podgurski and D. Perreault, "Submodule integrated distributed maximum power point tracking for solar photovoltaic applications," *IEEE Transactions on Power Electronics*, vol. 28, no. 6, pp. 2957–2967, 2013.

[5] Q. Li and P. Wolfs, "A review of the single phase photovoltaic module integrated converter topologies with three different dc link configurations," *IEEE Transaction on Power Electronics*, vol. 23, no. 3, pp. 1320–1333, 2008.

[6] R. Erickson and A. Rogers, "A microinverter for building-integrated photovoltaics," in *Proc. of the Applied Power Electronics Conference and Exposition*, pp. 911–917, 2009.

[7] A. Trubitsyn, B. Pierquet, A. Hayman, G. Gamache, C. Sullivan, and D. Perreault, "High-efficiency inverter for photovoltaic applications," in *Proc. of the Energy Conversion Congress and Exposition*, pp. 2803–2810, 2010.

[8] P. Shenoy, K. Kim, B. Johnson, and P. Krein, "Differential power processing for increased energy production and reliability of photovoltaic systems," *IEEE Transactions on Power Electronics*, vol. 28, no. 6, pp. 2968–2979, 2013.

[9] T. Shimizu, M. Hirakata, T. Kamezawa, and H. Watanabe, "Generation control circuit for photovoltaic modules," *IEEE Transactions on Power Electronics*, vol. 16, pp. 293 –300, May 2001.

[10] T. Shimizu, O. Hashimoto, and G. Kimura, "A novel high-performance utility-interactive photovoltaic inverter system," *IEEE Transaction on Power Electronics*, vol. 18, no. 2, pp. 704–711, 2003.

[11] J. Stauth, M. Seeman, and K. Kesarwani, "Resonant switched-capacitor converters for sub-module distributed photovoltaic power management," *IEEE Transactions on Power Electronics*, vol. 28, no. 3, pp. 1189–1198, 2013.

[12] C. Olalla, D. Clement, M. Rodriguez, and D. Maksimovic, "Architectures and control of submodule integrated dc-dc converters for photovoltaic applications," *IEEE Transactions on Power Electronics*, vol. 28, no. 6, pp. 2980–2997, 2013.

[13] S. Poshtkouhi, A. Biswas, and O. Trescases, "Dc-dc converter for high granularity, sub-string mppt in photovoltaic applications using a virtual-parallel connection," in *Proc. of the Applied Power Electronics Conference and Exposition*, pp. 86–92, 2012.

[14] S. Qin and R. C. Pilawa-Podgurski, "Sub-module differential power processing for photovoltaic applications," in *Proc. of the Applied Power Electronics Conference and Exposition*, pp. 101–108, 2013.

[15] H. Field and A. Gabor, "Cell binning method analysis to minimize mismatch losses and performance variation in si-based modules," in *Proc. of the Photovoltaic Specialists Conference*, pp. 418–421, 2002.

[16] C. E. Chamberlin, M. A. Rocheleau, M. W. Marshall, A. M. Reis, N. T. Coleman, and P. Lehman, "Comparison of pv module performance before and after 11 and 20 years of field exposure," in *Proc. of the Photovoltaic Specialists Conference*, pp. 101–105, 2011.

[17] B. Gharesifard and J. Cortes, "Distributed continuous-time convex optimization on weight-balanced digraphs," *IEEE Transactions on Automatic Control*, to appear, 2013.

[18] A. Peterchev and S. Sanders, "Quantization resolution and limit cycling in digitally controlled pwm converters," *IEEE Transactions on Power Electronics*, vol. 18, no. 1, pp. 301–308, 2003.

[19] C. Barth and R. Pilawa-Podgurski, "Implementation of dithering digital ripple correlation control," in *Proc. of the Workshop on Control, Modeling and Simulation in Power Electronics*, to appear, 2013.

[20] S. Qin, K. Kim, and R. Pilawa-Podgurski, "Laboratory emulation of a photovoltaic module for controllable insolation and realistic dynamic performance," in *Proc. of the Power and Energy Conference at Illinois*, pp. 23–29, 2013.